# 모서리 응력특이도의 영향을 포함한 고정 또는 자유 경계조건의 조합을 고려한 마름모꼴 평판의 휨 진동 해석

# Analysis of Flexural Vibration of Rhombic Plates with Combinations Clamped and Free Boundary Conditions Including the Effect of Corner Stress Singularities

김 주 우* 한 봉 구**
Kim, Joo Woo Han, Bong Koo

## 국문요약

본 논문에서는 고정 또는 자유 연단 조건의 모든 조합을 고려한 마름모꼴 평판의 휨 진동에 대한 엄밀한 해석방법을 제시한다. 본 논문의 주된 관점은 마름모꼴 평판 둔각모서리의 경계조건이 고정 또는 자유일 때 휨 응력의 특이도를 엄밀히 고려하여 해석하는 것이다. 고정 또는 자유인 모서리 응력 특이도의 중대한 영향력이 이해 될 수 있도록 충분히 큰 165° 둔각모서리를 갖는 마름모꼴 평판에 대하여 엄밀한 무차원 진동수와 수직변동변위의 전형적인 등고선을 제시하였다.

**주요어** : Ritz 방법, 자유진동, 모서리 응력 특이도, 마름모꼴 평판, 진동수, 휨

## ABSTRACT

An accurate method is presented for flexural vibrations of rhombic plates having all combinations of clamped and free edge conditions. The prime focus here is that the analysis explicitly considers the bending stress singularities that occur in the two opposite, *clamped-free* corners having obtuse angles of the rhombic plates. Accurate non-dimensional frequencies and normalized contours of the vibratory transverse displacement are presented for rhombic plates having a large enough obtuse angle of 165°, so that a significant influence of clamped-free corner stress singularities may be understood.

***Key words*** *: Ritz method, free vibration, corner stress singularity, rhombic plate, frequencies, bending*

## 1. Introduction

The evolution of the active research work on the free vibration of skewed (rhombic) plates with various combinations of clamped and free edge condition is described in a summarizing monograph[1] and in subsequent review articles.[2],[3],[4] More recent comprehensive treatments of the subject problem have been offered by Raju and Hinton[5], Ganeson and Rao.[6] Raju and Hinton[5] reported a large amount of vibration solutions for thin and thick, clamped skewed plates using nine-node isoparametric Mindlin plate finite elements. Ganeson and Rao[6] used a variational approach to examine the natural vibrations of thick skewed Mindlin plates with various combinations of clamped and free edge conditions, except those forming cantilevered ones. Liew

* 세명대학교 건축공학과 전임강사
** 정회원 · 서울산업대학교 구조공학과 교수
본 논문에 대한 토의를 6월 30일까지 학회로 보내 주시면 그 결과를 게재하겠습니다.

et. al.[7] examined the flexural vibrations of thick skewed plates having clamped-free edges using the Ritz method with the dynamical energies derived based on the Mindlin first-order shear deformation theory.

What is missing in the collective findings in the previous work[5),(6),(7)] is the effect of the bending stress singularities which exists at a clamped-free corner having an interior angle larger than 90° (i.e., obtuse). Analysts must explicitly consider such corner stress singularities in order to avoid erroneous results for highly skewed rhombic plates, particularly for the lower frequency modes. Fundamental information about the unbounded stresses which exist at obtuse corners in plate flexure problems involving static loads was explained in a paper by Williams.[8] Along these same lines, the importance of including re-entrant corner stress singularities on the natural vibration frequencies of cantilevered skewed plates[9] and simply supported rhombic plates[10] has been demonstrated in previous work.

In this paper, the bending stress singularities that exist at the two obtuse interior corners of rhombic plates having all possible combinations of clamped and free edges are taken into account explicitly. The dynamic energies are constructed using classical plate theory. Displacements are assumed as a mathematically complete set of algebraic polynomials and two admissible sets of corner functions. The latter functions account for the singular behavior of bending stresses at the two corners having obtuse angles. The Ritz method is used to minimize the dynamic energies to obtain upper bound approximate flexural frequencies and mode shapes as close to the exact ones, as sufficient numbers of polynomials and corner functions are retained. The accuracy of non-dimensional frequencies obtained by the present method is established through a convergence study explicitly showing the influence of the corner functions. Additional comparisons with previously published frequency data are made to elucidate the importance of considering corner stress singularities in obtaining accurate flexural vibration data for rhombic plates.

## 2. Method of analysis

Shown in Fig. 1 is a rhombic plate having typical length, $c$, and diagonal half-lengths, a and $b$, measured along the Cartesian axes, $x$ and $y$, respectively. The vibratory transverse displacement of the rhombic plate is $w = w(x, y, t)$, where $t$ is time. In using the Ritz method, one assumes that the rhombic plate undergoing undamped free vibration interchanges its

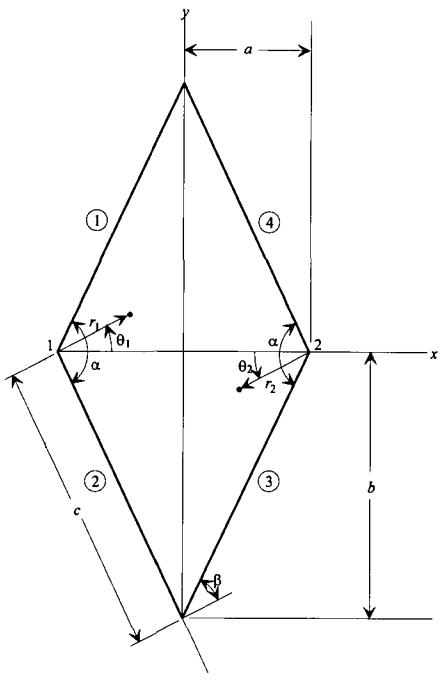


Fig. 1 Geometry of rhombic plate

dynamic energy from an uniquely potential condition at its maximum amplitude(zero velocity) to an uniquely kinetic condition at its maximum velocity(zero amplitude). At a circular frequency of vibration $\omega$, the temporal dependence of the transverse displacement $w$ is assumed to be simple harmonic:

$$w(x,y,t) = W(x,y)e^{j\omega t} \tag{1}$$

where $e$ is the exponential function and $j=\sqrt{-1}$.

Considering this assumption one can obtain the maximum strain energy $V_{\max}$ due to bending during a vibratory cycle upon taking $e^{jwt}$ as unity:

$$V_{\max} = \frac{D}{2}\iint_A \left[(\chi_x+\chi_y)^2 - 2(1-\nu)(\chi_x\chi_y+\chi_{xy}^2)\right]dA \tag{2}$$

where $dA = dxdy$, $D = Eh^3/12(1-\nu^2)$ is the flexural rigidity, $h$ is the plate thickness(not shown in Fig. 1), $E$ is Young's modulus, $\nu$ is Poisson's ratio, and $\chi_x$, $\chi_y$, and $\chi_{xy}$ are the maximum bending and twisting curvatures:

$$\chi_x = \frac{\partial^2 W}{\partial x^2}, \qquad \chi_y = \frac{\partial^2 W}{\partial y^2}, \qquad \chi_{xy} = \frac{\partial^2 W}{\partial x \partial y} \tag{2a}$$

Similarly, the maximum kinetic energy can be expressed as

$$T_{\max} = \frac{\rho\omega}{2}\iint_A W^2 dA \tag{3}$$

where $\rho$ is the mass per unit area of the plate.

In the present Ritz approach, displacement trial functions are assumed as

$$W(x,y) = W_p(x,y) + W_{c_1}(x,y) + W_{c_2}(x,y) \tag{4}$$

where $W_p$ is an admissible and mathematically complete set of algebraic polynomials, and $W_{c_1}$ and $W_{c_2}$ are two sets of corner functions, which adhere to the vanishing displacement and which account for the singular bending stress behavior at the obtuse corners 1 and 2, respectively(see Fig. 1). It should be noted that a clamped-free corner has singular bending stresses when the included angle ($\alpha$) formed by the two edges at corners 1 and 2 is larger than approximately 95° (i.e., obtuse).[11] No such unbounded stresses exist at either a clamped-clamped or free-free obtuse corner for $\alpha \leq 180°$.[11]

Four combinations of rhombic plate edge conditions are examined, which are hereafter described as *CFFF, CFFC, CFCF,* and *CFCC* (see Fig. 2, whereby only those edges which are free have been identified by the letter *F*). These edge conditions are identified according to the numbered edges shown in Fig. 1 (e.g., *C-F-C-F* corresponding to edges 1-2-3-4 as shown).

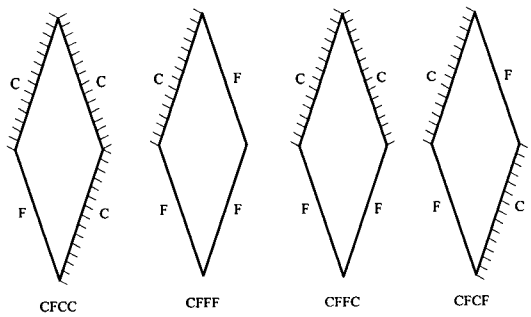


Fig. 2 Rhombic plates with clamped and edges

Let $G_j$ correspond to the equation of the $j$th edge of the rhombic plate shown in Fig. 1. Thus,

$$G_1 = b - y + \frac{b}{a}x, \qquad G_2 = b + y + \frac{b}{a}x,$$

$$G_3 = b + y - \frac{b}{a}x, \quad G_4 = b - y - \frac{b}{a}x \tag{5}$$

The polynomials $W_p$ are assumed as

*CFFF* plate: $W_p(x,y) = G_1^2\phi$ (6a)

*CFCF* plate: $W_p(x,y) = G_1^2 G_2^2\phi$ (6b)

*CFFC* plate: $W_p(x,y) = G_1^2 G_3^2\phi$ (6c)

*CFCC* plate: $W_p(x,y) = G_1^2 G_2^2 G_3^2\phi$ (6d)

where

$$\phi = \sum_m^M \sum_n^N A_{mn} x^m y^n \tag{6e}$$

and $A_{mn}$ are undetermined coefficients, $m$, $n$ = 0, 1, 2, ·, and $W_p$ satisfies the vanishing displacement and normal slope conditions on all the clamped boundaries as required. The corner functions $W_{c_i}$ ($i$=1,2) may be written as

*CFFF* plate: $W_{c_1}(x,y) = \xi_{1_k}$, $W_{c_2}(x,y) = 0$ (7a)

*CFCF* plate: $W_{c_1}(x,y) = G_3^2\xi_{1_k}$, $W_{c_2}(x,y) = G_1^2\xi_{2_k}$ (7b)

*CFFC* plate: $W_{c_1}(x,y) = G_4^2\xi_{1_k}$, $W_{c_2}(x,y) = G_1^2\xi_{2_k}$ (7c)

*CFCC* plate: $W_{c_1}(x,y) = G_3^2 G_4^2\xi_{1_k}$, $W_{c_2}(x,y) = 0$ (7d)

where

$$\xi_{i_k} = \sum_{k=1}^K B_{i_k} W_{c_{i_k}}^*(x,y) \tag{7e}$$

in which $B_{i_k}$ are arbitrary coefficients, and $W_{c_{i_k}}^*$ are biharmonic functions which satisfy the clamped-free boundary conditions along two radial edges of a sector plate domain.[11] For each of the plate edge conditions, $W_{c_{i_k}}^*$ is the $k^{\text{th}}$ function of the set:

*CFFF* and *CFCC* plates:

$$W_{c_{1_k}}^*(r_1,\theta_1) = r_1^{\lambda_k+1}[\sin(\lambda_k+1)\theta_1 + g_1\cos(\lambda_k+1)\theta_1 + g_2\sin(\lambda_k-1)\theta_1 + g_3\cos(\lambda_k-1)\theta_1] \tag{8a}$$

*CFCF* plate:

$$W_{c_{i_k}}^*(r_i,\theta_i) = r_i^{\lambda_k+1}[\sin(\lambda_k+1)\theta_i + g_1\cos(\lambda_k+1)\theta_i + g_2\sin(\lambda_k-1)\theta_i + g_3\cos(\lambda_k-1)\theta_i] \quad (i=1,2) \tag{8b}$$

*CFFC* plates:

$$W_{c_{1_k}}^*(r_1,\theta_1) = r_1^{\lambda_k+1}[\sin(\lambda_k+1)\theta_1 + g_1\cos(\lambda_k+1)\theta_1 + g_2\sin(\lambda_k-1)\theta_1 + g_3\cos(\lambda_k-1)\theta_1] \tag{8c}$$

$$W_{c_{2_k}}^*(r_2,\theta_2) = r_2^{\lambda_k+1}[\sin(\lambda_k+1)\theta_2 - g_1\cos(\lambda_k+1)\theta_2 + g_2\sin(\lambda_k-1)\theta_2 - g_3\cos(\lambda_k-1)\theta_2] \tag{8d}$$

with

$$g_1 = \frac{\mu_{1_k}}{\delta_k} \qquad g_2 = \frac{\mu_{2_k}}{\delta_k} \qquad g_1 = \frac{\mu_{3_k}}{\delta_k} \tag{9a}$$

$$\mu_{1_k} = (\lambda_k-1)\gamma_{2_k}\sin(\lambda_k+1)\frac{\alpha}{2} - (\lambda_k+1)\gamma_{1_k}\cos(\lambda_k+1)\frac{\alpha}{2}\sin(\lambda_k-1)\alpha + (\lambda_k-1)\gamma_{1_k}\sin(\lambda_k+1)\frac{\alpha}{2}\cos(\lambda_k-1)\alpha \tag{9b}$$

$$\mu_{2_k} = (\lambda_k+1)\left[\gamma_{1_k}\cos(\lambda_k-1)\frac{\alpha}{2} - \gamma_{2_k}\cos(\lambda_k-1)\frac{\alpha}{2}\cos(\lambda_k+1)\alpha - \gamma_{3_k}\sin(\lambda_k-1)\frac{\alpha}{2}\sin(\lambda_k+1)\alpha\right] \tag{9c}$$

$$\mu_{3_k} = (\lambda_k + 1)\Big[\gamma_{1_k}\sin(\lambda_k - 1)\frac{\alpha}{2} + \gamma_{2_k}\sin(\lambda_k - 1)\frac{\alpha}{2}\cos(\lambda_k + 1)\alpha - \gamma_{3_k}\cos(\lambda_k - 1)\frac{\alpha}{2}\sin(\lambda_k + 1)\alpha\Big] \tag{9d}$$

$$\delta_k = (\lambda_k - 1)\gamma_{2_k}\cos(\lambda_k + 1)\frac{\alpha}{2} - (\lambda_k + 1)\gamma_{1_k}\sin(\lambda_k + 1)\frac{\alpha}{2}\sin(\lambda_k - 1)\alpha - (\lambda_k - 1)\gamma_{1_k}\cos(\lambda_k + 1)\frac{\alpha}{2}\cos(\lambda_k - 1)\alpha \tag{9e}$$

in which

$$\gamma_{1_k} = \lambda_k(\nu - 1) + (3 + \nu), \quad \gamma_{2_k} = (\lambda_k + 1)(\nu - 1), \quad \gamma_{3_k} = (\lambda_k - 1)(\nu - 1) \tag{9f}$$

In Eqs. (8) and (9), the local polar coordinates $(r_i, \theta_i)$ originate at corners 1 and 2(Fig. 1), and $\alpha$ is the included angle of corner 1 and 2. In addition, the $\lambda_k$ are the roots of the characteristic equation:

$$\sin^2 \lambda_k \alpha = \frac{4}{(1-\nu)(3+\nu)} - \frac{1-\nu}{3+\nu}\lambda_k^2 \sin^2 \alpha \tag{10}$$

The functions $W^*_{c_{ik}}$, which are ordered by $\lambda_k$, are transformed to the global Cartesian coordinates ($x$, $y$) through the following relations:

$$r_1 = \left[(x+a)^2 + y^2\right]^{1/2} \qquad \theta_1 = \tan^{-1}\left[y(x+a)^{-1}\right]$$
$$r_2 = \left[(x-a)^2 + y^2\right]^{1/2} \qquad \theta_2 = \tan^{-1}\left[y(x-a)^{-1}\right] \tag{11}$$

The Ritz minimizing equations are formulated by substituting Eqs. (4)-(9) and (11) into (2) and (3) and taking the partial derivatives:

$$(V_{\max} - T_{\max})_{,A_{mn}} = 0, \qquad (V_{\max} - T_{\max})_{,B_{ik}} = 0 \tag{12}$$

The results in a set of Euler-Lagrange equations which are algebraic involving the constants $A_{mn}$ and $B_{i_k}$. The vanishing determinant of these equations yields a set of eigenvalues (natural frequencies), expressed in terms of the non-dimensional frequency parameter, $\omega a^2\sqrt{\rho/D}$, which is particularly suitable for the rhombic plate. The frequencies converge monotonically from above to the exact values, as sufficient number of terms in Eq. (4) are used.

Eigenvectors involving the coefficients constants $A_{mn}$ and $B_{i_k}$ may be determined in the usual manner by substituting the eigenvalues back into the homogeneous equations. Normalized contours of the associated mode shapes may be depicted on a $x$-$y$ grid in the rhombic plate domain once the eigenvectors are substituted into Eqs. (6e) and (7e).

## 3. Convergence studies and frequency comparison

All of the frequency and mode shape calculations in this work were performed on an IBM/RISC-6000 Model 970 powerserver with a Model 340 workstation cluster using double precision(14 significant digit) arithmetic. Table 1 describes a selected convergence study for the first six non-dimensional frequencies $\omega a^2\sqrt{\rho/D}$ of *CFCF* rhombic plates having $b/a$ = 3 (or $\alpha \cong 143^0$). The $(M+1)\times(N+1)$ number of polynomial terms ($W_p$) shown in Table 1 indicates $M+1$ terms retained in the $x$-direction and $N+1$ terms retained in the $y$-direction [see Eqs. (6)]. The $2K$ number of corner functions ($W_c = W_{c_1} + W_{c_2}$) define $K$ corner functions used in Eqs. (7) for each of corners 1 and 2. Poissons ratio ($\nu$) has been set to 0.3 in all calculations.

Table 1 Convergence of frequency parameters $\omega a^2\sqrt{\rho/D}$ for a *CFCF* rhombic plate ($b/a$ = 3)

| Mode No. | Corner Functions ($W_c$) | ($M$+1)x($N$+1) polynomial terms ($Wp$) | | | | | | |
|---|---|---|---|---|---|---|---|---|
| | | 8×8 | 9×9 | 10×10 | 11×11 | 12×12 | 13×13 | 14×14 |
| 1 | 0 | 4.6725 | 4.6352 | 4.6068 | 4.5882 | 4.5757 | 4.5647 | 4.5592 |
| | 4 | 4.5385 | 4.5336 | 4.5327 | 4.5319 | 4.5317 | 4.5315 | 4.5315 |
| | 8 | 4.5340 | 4.5324 | 4.5320 | 4.5316 | 4.5315 | 4.5315 | 4.5314 |
| | 12 | 4.5330 | 4.5320 | 4.5318 | 4.5315 | 4.5315 | 4.5314 | 4.5314 |
| | 16 | 4.5318 | 4.5316 | 4.5314 | 4.5312 | --- | --- | --- |
| | 20 | 4.5317 | 4.5314 | --- | --- | --- | --- | --- |
| 2 | 0 | 4.7862 | 4.7273 | 4.6933 | 4.6658 | 4.6455 | 4.6320 | 4.6193 |
| | 4 | 4.5790 | 4.5770 | 4.5760 | 4.5755 | 4.5752 | 4.5751 | 4.5750 |
| | 8 | 4.5765 | 4.5758 | 4.5754 | 4.5752 | 4.5751 | 4.5750 | 4.5750 |
| | 12 | 4.5760 | 4.5756 | 4.5753 | 4.5751 | 4.5750 | 4.5750 | 4.5749 |
| | 16 | 4.5758 | 4.5753 | 4.5751 | 4.5749 | --- | --- | --- |
| | 20 | 4.5751 | 4.5737 | --- | --- | --- | --- | --- |
| 3 | 0 | 7.6092 | 7.5964 | 7.5929 | 7.5901 | 7.5875 | 7.5866 | 7.5845 |
| | 4 | 7.5779 | 7.5717 | 7.5709 | 7.5705 | 7.5702 | 7.5701 | 7.5701 |
| | 8 | 7.5728 | 7.5708 | 7.5704 | 7.5703 | 7.5701 | 7.5700 | 7.5700 |
| | 12 | 7.5711 | 7.5701 | 7.5701 | 7.5701 | 7.5700 | 7.5700 | 7.5700 |
| | 16 | 7.5704 | 7.5701 | 7.5700 | 5.5697 | --- | --- | --- |
| | 20 | 7.5701 | 7.5698 | --- | --- | --- | --- | --- |
| 4 | 0 | 10.094 | 10.050 | 9.9745 | 9.9533 | 9.9311 | 9.9199 | 9.9069 |
| | 4 | 9.9190 | 9.9091 | 9.8678 | 9.8672 | 9.8648 | 9.8646 | 9.8644 |
| | 8 | 9.9108 | 9.9030 | 9.8665 | 9.8663 | 9.8645 | 9.8644 | 9.8643 |
| | 12 | 9.8759 | 9.8689 | 9.8649 | 9.8647 | 9.8644 | 9.8643 | 9.8643 |
| | 16 | 9.8722 | 9.8669 | 9.8648 | 9.8645 | --- | --- | --- |
| | 20 | 9.8675 | 9.8644 | --- | --- | --- | --- | --- |
| 5 | 0 | 13.282 | 12.623 | 12.477 | 12.355 | 12.296 | 12.257 | 12.228 |
| | 4 | 12.594 | 12.215 | 12.168 | 12.101 | 12.097 | 12.090 | 12.089 |
| | 8 | 12.386 | 12.185 | 12.141 | 12.098 | 12.094 | 12.089 | 12.089 |
| | 12 | 12.289 | 12.153 | 12.131 | 12.095 | 12.094 | 12.089 | 12.089 |
| | 16 | 12.119 | 12.101 | 12.091 | 12.090 | --- | --- | --- |
| | 20 | 12.115 | 12.095 | --- | --- | --- | --- | --- |
| 6 | 0 | 15.240 | 15.078 | 14.983 | 14.910 | 14.861 | 14.828 | 14.799 |
| | 4 | 14.747 | 14.728 | 14.709 | 14.702 | 14.699 | 14.697 | 14.696 |
| | 8 | 14.731 | 14.719 | 14.705 | 14.700 | 14.698 | 14.697 | 14.696 |
| | 12 | 14.726 | 14.715 | 14.704 | 14.700 | 14.698 | 14.697 | 14.696 |
| | 16 | 14.721 | 14.707 | 14.700 | 14.697 | --- | --- | --- |
| | 20 | 14.703 | 14.695 | --- | --- | --- | --- | --- |

--- no results due to matrix ill-conditioning

The convergence of frequencies in Table 1 shows that by using polynomial terms alone typically results in a relatively slow rate of upper bound convergence of $\omega a^2\sqrt{\rho/D}$ values for the *CFCF* rhombic plates. Whereas, the rate of convergence of $\omega a^2\sqrt{\rho/D}$ is significantly accelerated when a few corner functions are added to the polynomials (depending on the mode number and plate boundary conditions). For example, using 100 polynomial terms (10

$\times 10$) without corner functions to represent the fundamental(lowest frequency) mode of an *CFCF* plate with $b/a$=3 yields an error of approximately 1.7% in the predicted frequency. Increasing to 196 polynomial terms ($14\times 14$) still results in an error of 0.6%. When the trial set of 100 polynomials are supplemented with 4 corner functions the predicted frequency error reduces to a negligible amount of 0.03%. Indeed, for the *CFCF* plate (Table 1), the exact $\omega a^2\sqrt{\rho/D}$ for the lowest frequency mode is achieved to four significant digits with a solution sizes as small as $9\times 9+20$. It should be noted that the *CFCF* case is the one of the most challenging convergence studies among the four cases analyzed here, and that levels of solution accuracy similar to that exhibited above may be seen in all modes of the *CFCC*, *CFFF*, and *CFFC* plates.

For the *CFCF*, *CFCC*, *CFFF*, and *CFFC* rhombic plates, large gradients of the vibratory stresses exist at the obtuse *CF* corners. The vibratory stresses are, however, bounded near the *CC* and *FF* corners. Previous studies[11] have shown that the moment stresses are unbounded at a *CF* corner when approximately $\alpha > 95°$ and at a CC and *FF* corner when $\alpha > 180°$, which at the latter is valid for sectorial rather than rhombic plates.

Table 2 is a summary of accurate rhombic plate frequencies for the four possible combinations of clamped and free edges. Listed therein are the first five non-dimensional frequencies $\omega c^2\sqrt{\rho/D}$ ($c$ being the side length, as shown in Fig. 1) of the *CFCF*, *CFCC*, *CFFF*, and *CFFC* rhombic plates having skew angles $\beta$(corner angles $\alpha$)=15°(105°), 30°(120°), 45°(135°), 60°(150°), and 75°(165°). Accurate qualitative modeling of the singular stress phenomena dictates the for large $\beta(\alpha)$, a considerable number of corner functions are required at corners 1 and 2 for the *CFCF* and *CFFC* rhombic plates, and at corner 1 for the *CFCC* and *CFFF* plates. Sufficient numbers of polynomials ( $W_p$) and corner functions ( $W_c$) were used to yield at least five significant digit accuracy of the frequencies shown in Table 2. The converged solution sizes employed are summarized in Table 3.

It may be seen in Table 2 that as the side length ($c$) remains constant $\omega c^2\sqrt{\rho/D}$ increases with increasing $\beta$, and that the highest frequency values are obtained for the *CFCC* plates, which is to be expected. For all plates, substantial changes in $\omega c^2\sqrt{\rho/D}$ traceable to plate skewness are most distinguishable for $45° \le \beta \le 75°$, where one can observe increasingly greater frequency changes as the mode number increases.

Frequency solutions for the square plates ($\alpha$=90°, $\beta$=0°), which have been calculated in the present analysis with no corner functions (see Table 3), are lower upper-bound $\omega c^2\sqrt{\rho/D}$ values compared to those values reported in reference 12, which were obtained by employing the Ritz method with beam eigenfunction approximation of the plates normal displacement. Non-dimensional frequencies obtained by the present method for the *CFCF* and *CFFF* plates are compared in Table 4 with those reported in a first-order shear deformable Mindlin plate Ritz analysis.[7] In the latter, the plate thickness ratio ($b/h$) was set to 1000, which is considered as very thin. As expected for the square *CFCF* and *CFFF* plates ($\alpha$=90°, $\beta$=0°), both the present and shear deformable approximate methods converge to the exact solution. Moreover, there appears to be close agreement between the $\omega c^2\sqrt{\rho/D}$ values for $\alpha$=105° ($\beta$=15°). For $\alpha > 105$

Table 2 Frequency parameters $\omega c^2\sqrt{\rho/D}$ for rhombic plates with clamped and free edge conditions

| Skew Angle($\beta$) | $\alpha$ | b/a | Mode No. | CFCF | CFCC | CFFF | CFFC |
|---|---|---|---|---|---|---|---|
| 0° | 90° | 1.000 | 1 | 22.168 | 23.924 | 3.4711 | 6.9191 |
| | | | | (22.272) | (24.020) | (3.4917) | (6.9421) |
| | | | 2 | 26.408 | 40.000 | 8.5073 | 23.902 |
| | | | | (26.529) | (40.039) | (8.5246) | (24.034) |
| | | | 3 | 43.596 | 63.229 | 21.286 | 26.585 |
| | | | | (43.664) | (63.493) | (21.429) | (26.681) |
| | | | 4 | 61.177 | 76.712 | 27.199 | 47.649 |
| | | | | (61.466) | (76.761) | (27.331) | (47.785) |
| | | | 5 | 67.181 | 80.579 | 30.959 | 62.705 |
| | | | | (67.549) | (80.713) | (31.111) | (63.039) |
| 15° | 105° | 1.303 | 1 | 23.342 | 25.049 | 3.5813 | 6.4436 |
| | | | 2 | 27.324 | 41.689 | 8.6968 | 24.782 |
| | | | 3 | 44.825 | 66.697 | 22.229 | 25.254 |
| | | | 4 | 64.488 | 76.150 | 26.333 | 47.510 |
| | | | 5 | 70.349 | 88.624 | 33.861 | 64.276 |
| 30° | 120° | 1.732 | 1 | 27.387 | 28.876 | 3.9278 | 6.2414 |
| | | | 2 | 30.531 | 47.866 | 9.4098 | 24.742 |
| | | | 3 | 49.476 | 76.723 | 25.286 | 28.386 |
| | | | 4 | 73.893 | 83.714 | 25.931 | 49.360 |
| | | | 5 | 80.869 | 109.50 | 41.331 | 71.340 |
| 45° | 135° | 2.414 | 1 | 36.384 | 37.254 | 4.5051 | 6.2066 |
| | | | 2 | 37.961 | 63.242 | 11.247 | 25.735 |
| | | | 3 | 61.671 | 92.993 | 26.967 | 34.303 |
| | | | 4 | 86.685 | 112.23 | 31.503 | 55.637 |
| | | | 5 | 102.16 | 139.05 | 50.710 | 82.870 |
| 60° | 150° | 3.732 | 1 | 56.857 | 57.225 | 5.2427 | 6.2912 |
| | | | 2 | 57.460 | 102.94 | 16.022 | 26.990 |
| | | | 3 | 96.556 | 135.85 | 30.357 | 46.567 |
| | | | 4 | 115.58 | 182.29 | 45.290 | 63.765 |
| | | | 5 | 145.13 | 196.25 | 59.035 | 107.17 |
| 75° | 165° | 7.596 | 1 | 135.95 | 137.54 | 6.0231 | 6.4933 |
| | | | 2 | 138.85 | 230.00 | 24.821 | 28.171 |
| | | | 3 | 228.56 | 331.67 | 48.746 | 68.508 |
| | | | 4 | 230.25 | 412.39 | 72.566 | 83.815 |
| | | | 5 | 319.04 | 508.69 | 95.380 | 126.46 |

Results in parentheses cf. Leissa[12]

($\beta$ > 15), however, the influence of the corner stress singularities becomes more significant, hence, the results of Liew et. al.[7] are, in most instances, slightly higher upper bounds on the exact $\omega c^2\sqrt{\rho/D}$ values compared to those obtained by the present method, especially for plates having large b. When the bending stress singularities are considered, a first-order (Mindlin) shear deformable analysis[7] should in principle yield lower $\omega c^2\sqrt{\rho/D}$ values than the present classical thin-plate solutions. Judging from the frequency comparison in Table 4, one must conclude that one must consider Williams-type corner stress singularities not only for classically thin-plates but for shear deformable ones also.

Table 3 Number of polynomial and corner function terms required of the five significant figure frequency convergence of Table 2

| Edges | $\beta$ (degrees) | Polynomial terms | Corner functions |
|---|---|---|---|
| CFCF | 0 | 14×14 | 2 |
| | 15, 30 45 | 14×14 | 8 |
| | 60 | 14×14 | 12 |
| | 75 | 14×14 | 20 |
| CFCC | 0 | 14×14 | 0 |
| | 15, 30 | 14×14 | 4 |
| | 45 | 14×14 | 6 |
| | 60 | 14×14 | 8 |
| | 75 | 14×14 | 10 |
| CFFF | 0 | 18×18 | 0 |
| | 15, 45 | 14×14 | 4 |
| | 30, 60 | 14×14 | 6 |
| | 75 | 14×14 | 8 |
| CFFC | 0 | 14×14 | 2 |
| | 15, 30 | 14×14 | 4 |
| | 45 | 14×14 | 8 |
| | 60 | 14×14 | 12 |
| | 75 | 14×14 | 16 |

## 4. Vibratory displacement contours

Depicted in Figs. 3 and 4 are the vibratory transverse displacement contours corresponding to the least upper bound frequency data for the first six modes. The displacement contours in Figs. 3 and 4 are normalized with respect to the maximum displacement component (i.e., $-1 \le W/W_{\max} \le 1$). Nondimensional frequencies $\omega a^2\sqrt{\rho/D}$ shown in Figs. 3 and 4 correspond to the converged values for the rhombic plates having $b/a$=3 (or $\alpha \cong 143^\circ$). For clarity in Figs. 3 and 4, the nodal patterns (lines of zero displacement during the vibratory motion) are described by the slightly darker contour lines.

Table 4 Comparison of frequency parameters $\omega c^2\sqrt{\rho/D}$ for rhombic plates with CFCF and CFFF edge conditions

| Skew Angle ($\beta$) | $\alpha$ | $\beta/a$ | Mode No. | CFCF | | CFFF | |
|---|---|---|---|---|---|---|---|
| | | | | Present Work | Liew *et al.* [7] | Present Work | Liew *et al.* [7] |
| 00 | 900 | 1.000 | 1 | 22.168 | 22.169 | 3.4711 | 3.4711 |
| | | | 2 | 26.408 | 26.410 | 8.5073 | 8.5076 |
| | | | 3 | 43.596 | 43.599 | 21.286 | 21.287 |
| | | | 4 | 61.177 | 61.181 | 27.199 | 27.199 |
| | | | 5 | 67.181 | 67.189 | 30.959 | 30.959 |
| 150 | 1050 | 1.303 | 1 | 23.342 | 23.348 | 3.5831 | 3.5837 |
| | | | 2 | 27.324 | 27.331 | 8.6968 | 8.7918 |
| | | | 3 | 44.825 | 44.827 | 22.229 | 22.237 |
| | | | 4 | 64.488 | 64.500 | 26.333 | 27.605 |
| | | | 5 | 70.349 | 70.366 | 33.861 | 34.182 |
| 300 | 1200 | 1.732 | 1 | 27.387 | 27.401 | 3.9278 | 3.9311 |
| | | | 2 | 30.351 | 30.548 | 9.4098 | 9.4126 |
| | | | 3 | 49.476 | 49.500 | 25.286 | 25.297 |
| | | | 4 | 73.893 | 73.921 | 25.931 | 25.934 |
| | | | 5 | 80.869 | 80.934 | 41.331 | 41.341 |
| 450 | 1350 | 2.414 | 1 | 36.384 | 36.451 | 4.5051 | 4.5114 |
| | | | 2 | 37.961 | 38.073 | 11.247 | 11.255 |
| | | | 3 | 61.671 | 61.785 | 26.967 | 27.000 |
| | | | 4 | 86.685 | 86.799 | 31.503 | 31.565 |
| | | | 5 | 102.16 | 102.71 | 50.710 | 50.715 |
| 600 | 1500 | 3.732 | 1 | 56.857 | 57.820 | 5.2427 | 5.2763 |
| | | | 2 | 57.460 | 58.235 | 16.022 | 16.097 |
| | | | 3 | 96.556 | 96.860 | 30.357 | 30.658 |
| | | | 4 | 115.58 | 116.62 | 45.290 | 45.603 |
| | | | 5 | 145.13 | 147.15 | 59.035 | 59.324 |
| 750 | 1650 | 7.596 | 1 | 135.95 | --- | 6.0231 | --- |
| | | | 2 | 138.85 | --- | 24.821 | --- |
| | | | 3 | 228.56 | --- | 48.746 | --- |
| | | | 4 | 230.25 | --- | 72.566 | --- |
| | | | 5 | 319.04 | --- | 95.380 | --- |

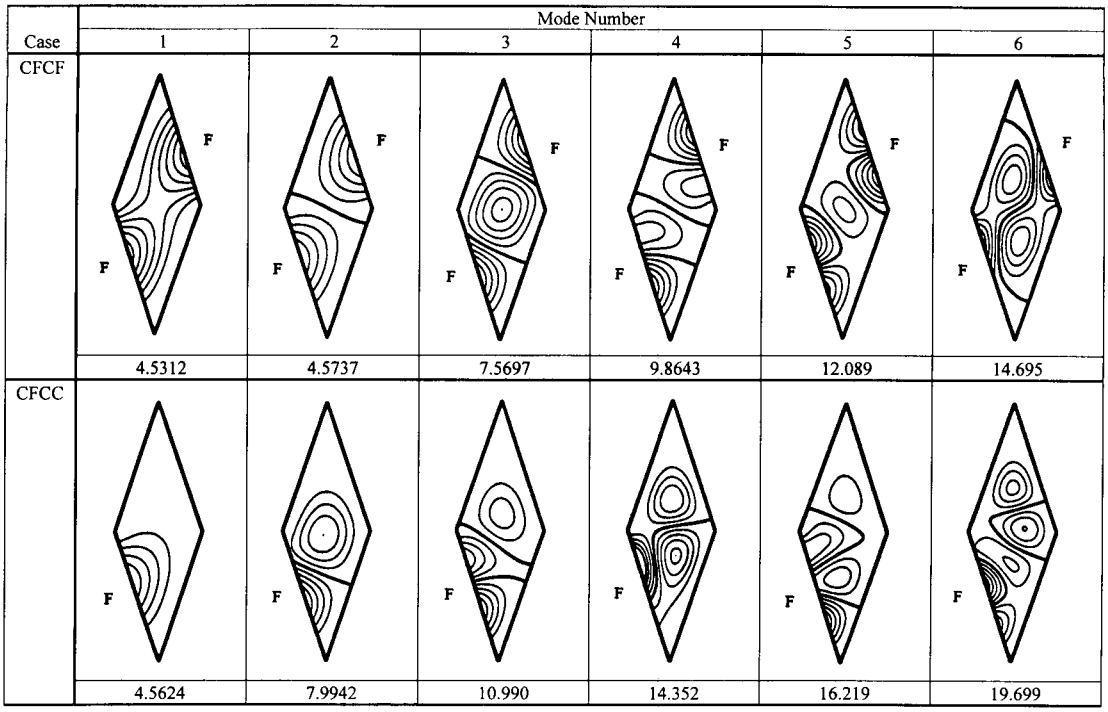


Fig. 3 Normalized transverse displacement contours($W/W_{max}$) for the first six modes of *CFCF* and *CFCC* rhombic plates($b/a$=3)

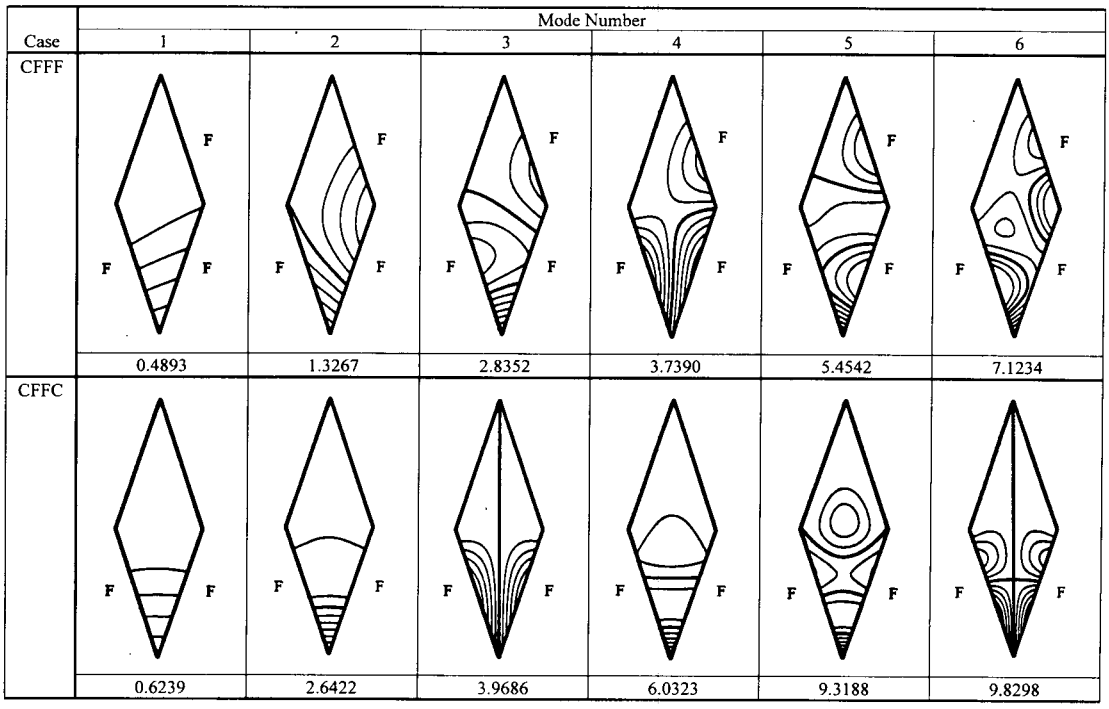


Fig. 4 Normalized transverse displacement contours($W/W_{max}$) for the first six modes of *CFFF* and *CFFC* rhombic plates($b/a$=3)

When one considers the normal symmetry with respect to the *y*-axes of the *CFFC* rhombic plate (see Fig. 4), modes 3 and 6 are also the first known nodal patterns of a *CFS* isosceles triangular plates (*b/a*=3) having stress singularities at the vertex of their apex angle. This is because the significant straight node line lying along the *y*-symmetry axis duplicate a simply supported edge (with vanishing vibratory moments). No such stress singularities are present at the *FS* and *SC* acute base angles.

## 5. Concluding remarks

The primary contribution here is an alternative for obtaining accurate upper bound solutions for free vibrations of classically thin, skew rhombic plates with clamped and free edges, while explicitly include stress singularities at the two obtuse clamped-free corners. The dynamical energies of the plate have been extremized via the Ritz method with the transverse displacement field approximated by mathematically complete polynomials and admissible corner functions that account for the unbounded stresses at the obtuse clamped-free corners. The accuracy of the assumed displacement field has been validated by means of a convergence table. Here, it has been shown that the convergence of solution is enhanced when the hybrid trial sets of polynomials and corner functions are simultaneously utilized.

The accurate frequencies and mode shapes for highly skewed ($\beta$ > 45°) rhombic plates presented herein may serve as benchmarks for comparison with future solutions offered by other investigators. A point of methodological procedure is that investigators using continuum-based and discrete element-based formulations will have difficulty in calculating accurate solutions to the title problem unless they explicitly consider in the assumed displacement or stress fields the moment singularities at the obtuse clamped-free corners.

## References


1. Leissa, A. W., "Vibration of plates," NASA SP-160, *Acoustical Society of America*, U.S. Government Printing Office, 1969. Reprinted, 1993.
2. Leissa, A. W., "Recent research in plate vibrations: classical theory," *Shock and Vibration Digest*, Vol. 9, No. 10, 1977, pp. 13-24.
3. Leissa, A. W., "Plate vibration research 1976-1980: classical theory," *Shock and Vibration Digest*, Vol. 13, No. 9, 1981, pp. 11-22.
4. Leissa, A. W., "Recent studies in plate vibrations: 1981-1985: part I classical theory," *Shock and Vibration Digest*, Vol. 19, No. 2, 1987, pp. 11-18.
5. Kanaka Raju, K. and Hinton, E., "Natural frequencies and modes of rhombic Mindlin plates," *Earthquake Engineering and Structural Dynamics*, Vol. 8, 1980, pp. 55-62.
6. Ganesan, N. and Nagaraja Rao, S., "Vibration analysis of moderately thick skew plates by a variational approach," *Journal of Sound and Vibration*, Vol. 101, No. 1, 1985, pp. 117-119.
7. Liew, K. M., Xiang, Y., Kitipornchai, S., and Wang, C. M., "Vibration of thick skew plates based on Mindlin shear deformation plate theory," *Journal of Sound and Vibration*, Vol. 168, No. 1, 1993, pp. 39-69.

8. Williams, M. L., "Surface stress singularities resulting from various boundary conditions in angular corners of plates under bending," *Proceedings of the first U.S. National Congress of Applied Mechanics*, 1951, pp. 325-329.
9. McGee, O. G., Leissa, A. W., and Huang, C. S., "Vibration of cantilevered skewed plates with corner stress singularities," *International Journal for Numerical Methods in Engineering*, Vol. 35, No. 2, 1992, pp. 409-424.
10. Huang, C. S., McGee, O. G., Leissa, A. W., and Kim, J. W., "Accurate vibration analysis of simply supported rhombic plates by considering stress singularities," *Journal of Vibration and Acoustics*, ASME, Vol. 151, 1995, pp. 245-251.
11. Leissa, A. W., McGee, O. G., and Huang, C. S., "Vibration of sectorial plates having corner stress singularities," *Journal of Applied Mechanics*, Vol. 60, No. 2, 1993, pp. 134-140.
12. Leissa, A. W., "The free vibration of rectangular plates," *Journal of Sound and Vibration*, Vol. 31, No. 3, 1971, pp. 257-293.